THE PLANT CELL

The Plant Cell, 2024, **36**, 4132–4142

https://doi.org/10.1093/plcell/koae143
Advance access publication 13 May 2024
Research Article

Alternative electron pathways of photosynthesis power green algal CO_2 capture

Gilles Peltier,[1] Carolyne Stoffel,[2] Justin Findinier,[2] Sai Kiran Madireddi,[2] Ousmane Dao,[1] Virginie Epting,[1] Amélie Morin,[1] Arthur Grossman,[2,3,4] Yonghua Li-Beisson,[1] and Adrien Burlacot[2,3,4,*]

[1]Aix Marseille Univ, CEA, CNRS, Institut de Biosciences et Biotechnologies Aix-Marseille, CEA Cadarache, 13108 Saint Paul-lez-Durance, France
[2]Department of Plant Biology, The Carnegie Institution for Science, Stanford, CA 94305, USA
[3]Department of Biology, Stanford University, Stanford, CA 94305, USA
[4]Biosphere Science and Engineering Division, The Carnegie Institution for Science, Stanford, CA 94305, USA
*Author for correspondence: aburlacot@carnegiescience.edu
The author responsible for distribution of materials integral to the findings presented in this article in accordance with the policy described in the Instructions for Authors (https://academic.oup.com/plcell/pages/General-Instructions) is: Adrien Burlacot (aburlacot@carnegiescience.edu).

Abstract

Microalgae contribute to about half of global net photosynthesis, which converts sunlight into the chemical energy (ATP and NADPH) used to transform CO_2 into biomass. Alternative electron pathways of photosynthesis have been proposed to generate additional ATP that is required to sustain CO_2 fixation. However, the relative importance of each alternative pathway remains elusive. Here, we dissect and quantify the contribution of cyclic, pseudo-cyclic, and chloroplast-to-mitochondrion electron flows for their ability to sustain net photosynthesis in the microalga *Chlamydomonas reinhardtii*. We show that (i) each alternative pathway can provide sufficient additional energy to sustain high CO_2 fixation rates, (ii) the alternative pathways exhibit cross-compensation, and (iii) the activity of at least one of the three alternative pathways is necessary to sustain photosynthesis. We further show that all pathways have very different efficiencies at energizing CO_2 fixation, with the chloroplast–mitochondrion interaction being the most efficient. Overall, our data lay bioenergetic foundations for biotechnological strategies to improve CO_2 capture and fixation.

Introduction

Oxygenic photosynthesis is the main process responsible for the carbon input into ecosystems on Earth, with net CO_2 fixation by photosynthesis representing more than 10 times anthropogenic CO_2 emissions (IPCC 2021). During photosynthesis, CO_2 fixation is powered by the combined action of PSI and PSII, establishing a linear electron flow (LEF) that produces reducing power (NADPH) and a trans-thylakoid proton motive force (*pmf*) used to generate ATP. Both ATP and NADPH fuel the CO_2 fixation via the Calvin–Benson–Bassham (CBB) cycle and the further processing of the glyceraldehyde-3-phosphate to regenerate ribulose-1,5-bisphosphate and produce building blocks used for the elaboration of biomass (Johnson and Alric 2013). However, given the insufficiency of LEF to generate an adequate *pmf* and the conversion efficiency of the chloroplastic ATP-synthase (ATPase), it has been long recognized that LEF only generates 85% of the theoretical ATP requirements of the CBB cycle (Allen 2003).

Cyclic electron flow (CEF), which recycles reducing equivalents around PSI, and pseudo-cyclic electron flow (PCEF), which reduces molecular O_2 at the acceptor side of PSI (Fig. 1), were proposed to contribute to the production of extra ATP during photosynthesis (Arnon 1959, 1984). In most angiosperms and mosses, CEF entails two main pathways, one involving the PROTON GRADIENT REGULATION 5 (PGR5) (Munekage et al. 2002) and PGR-LIKE 1 proteins (DalCorso et al. 2008) and another involving the plastidial NAD(P)H dehydrogenase-like (NDH) complex NDH-1 (Joët et al. 2001; Munekage et al. 2004). In many green microalgae, the plastidial NDH-1 complex is absent (Peltier et al. 2016) although they still have two CEF pathways, one controlled by PGRL1 and PGR5 (Tolleter et al. 2011; Johnson et al. 2014) and the other involving the plastidial NAD(P)H dehydrogenase Nda2 (Jans et al. 2008; Desplats et al. 2009; Saroussi et al. 2016). Since the Nda2 pathway is mostly active during nitrogen deprivation (Peltier and Schmidt 1991; Saroussi et al. 2016), hereafter, CEF refers to the PGRL1/PGR5-controlled CEF. PCEF involves flavodiiron proteins (FLVs) that catalyze O_2 photoreduction at the PSI acceptor side (Fig. 1) in cyanobacteria (Helman et al. 2003; Allahverdiyeva et al. 2013), green microalgae (Chaux et al. 2017), mosses (Gerotto et al. 2016), liverwort (Shimakawa et al. 2017), and gymnosperms (Ilík et al. 2017).

Another mechanism that can supply ATP to photosynthesis involves metabolic cooperation between chloroplasts and mitochondria (Raghavendra and Padmasree 2003). Reducing power generated within the chloroplast is transferred to mitochondria by metabolic shuttles where it is converted to ATP by the mitochondrial respiratory chain and might be shuttled back to the cytosol and the chloroplast (Fig. 1). Such a cooperation, called chloroplast-to-mitochondrion electron flow (CMEF), was first evidenced from the restoration of photoautotrophic growth in a mutant of the green microalgae *Chlamydomonas* (*Chlamydomonas*

Received March 08, 2024. Accepted April 9, 2024
© The Author(s) 2024. Published by Oxford University Press on behalf of American Society of Plant Biologists.
This is an Open Access article distributed under the terms of the Creative Commons Attribution-NonCommercial-NoDerivs licence (https://creativecommons.org/licenses/by-nc-nd/4.0/), which permits non-commercial reproduction and distribution of the work, in any medium, provided the original work is not altered or transformed in any way, and that the work is properly cited. For commercial re-use, please contact reprints@oup.com for reprints and translation rights for reprints. All other permissions can be obtained through our RightsLink service via the Permissions link on the article page on our site—for further information please contact journals.permissions@oup.com.

reinhardtii) deficient in the plastidial ATPase (Lemaire et al. 1988). Similar cooperation was later suggested from studies of *Chlamydomonas* mutants affected in mitochondrial respiration (Cardol et al. 2003) or in CEF (Dang et al. 2014) and was also observed in the moss *Physcomitrium patens* (Mellon et al. 2021) and in diatoms (Bailleul et al. 2015).

It is generally considered that both PCEF and CMEF act essentially as electron valves, operating either transiently in the case of PCEF to alleviate excess electrons generated by photosynthesis under light fluctuating regimes (Alric and Johnson 2017; Chaux et al. 2017; Alboresi et al. 2019) or more continuously for CMEF under high light stress (Kaye et al. 2019). Although, in *Chlamydomonas*, CMEF, PCEF, and CEF have been recently shown to all contribute to supply energy to the CO_2 concentrating mechanism (CCM) (Burlacot et al. 2022), evidence for their role in powering the CBB cycle and downstream carbon metabolism processes is scarce.

In this work, we show that each pathway (CEF, PCEF, and CMEF) has the capacity to sustain net CO_2 fixation to varying degrees and can compensate for the absence of the other pathways, whereas CO_2 fixation is completely abolished in the absence of all three pathways. Moreover, we introduce a method to quantify the efficiency and capacity of each pathway and use it to show that CMEF is by far the most efficient at energizing CO_2 fixation. We further discuss our data in relation to the relative contribution and efficiency of the different alternative pathways to the net primary productivity of terrestrial and oceanic ecosystems.

Results

Net photosynthesis fully relies on mitochondrial respiration when PCEF and CEF are impaired

To test whether PCEF and CEF are required for maximal net photosynthesis (V_{Max}), we first measured photosynthetic O_2 exchange rates using membrane inlet mass spectrometry (MIMS) (Burlacot et al. 2020) in air-grown *Chlamydomonas* control cells (wild types [WTs] 2 and 3) and mutants impaired in both CEF and PCEF (*pgrl1 flvB-1* and -3) (Burlacot et al. 2022). Since the *pgrl1* and *flvB* mutants are both affected in the functioning of the CCM (Burlacot et al. 2022), photosynthesis measurements were performed in the presence of a saturating concentration of inorganic carbon (C_i) when the CCM is inactive. As previously reported (Burlacot et al. 2022), *pgrl1 flvB* double mutants can perform photosynthesis at maximum rates comparable to the single *pgrl1* or *flvB* mutants and to the parental and sibling control strains (Fig. 2; Supplementary Figs. S1A, S2, and S3), showing that neither CEF nor PCEF is essential to reach V_{Max}. To test a possible contribution of mitochondrial respiration to photosynthesis, *pgrl1 flvB* double mutants were treated with myxothiazol (Myxo) and salicylhydroxamic acid (SHAM), inhibitors of mitochondrial electron transport, respectively acting on complex III and the alternative oxidases (AOX) (Fig. 1) (Schonbaum et al. 1971; von Jagow and Link 1986). While the addition of both respiratory inhibitors had a small impact (about 10% to 20% decrease) on the V_{Max} of control strains (Fig. 2, A and C; Supplementary Figs. S1A, S2, and S3), they completely abolished photosynthesis in *pgrl1 flvB* double mutants (Fig. 2, B and C; Supplementary Figs. S1 and S2).

In *Chlamydomonas*, the cellular location of mitochondria depends on the CO_2 supply, with the mitochondria located at the cell periphery in low CO_2-grown cells and mostly inside the chloroplast cup in high CO_2 (Geraghty and Spalding 1996) (Fig. 2, E and F). Since this location might affect CMEF (Burlacot and Peltier 2023), we sought to examine the involvement of the mitochondrial subcellular localization on the role of CMEF. As with air-grown cells, mitochondrial inhibitors fully stopped net photosynthesis on 2% CO_2-grown *pgrl1 flvB* mutants while having a marginal effect (about 10% to 20% decrease) on the control strains (Fig. 2D; Supplementary Fig. S4). To control the location of the mitochondria in the different strains, we visualized the spatial distribution of an expressed, mitochondrion-targeted fluorophore (Clover). There was similar relocalization of mitochondria depending on the CO_2 supply during growth (at periphery under very low CO_2) of both the single and double mutants and a control strain (Fig. 2, E and F; Supplementary Fig. S5). We conclude from these experiments that the absence of CEF, PCEF, and CMEF abolishes net photosynthesis. Furthermore, in the absence of both CEF and PCEF, near WT levels of photosynthesis can be achieved that fully rely on CMEF, which does not appear to rely on the spatial distribution of the mitochondria.

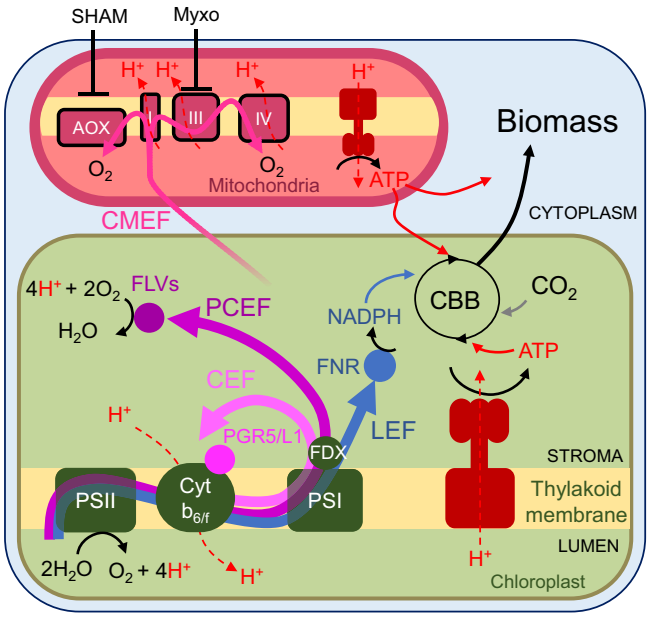

Figure 1. Electron transport pathways operating during oxygenic photosynthesis and their role in ATP generation. LEF (blue solid arrow) operates from PSII to PSI and reduces $NADP^+$ to NADPH using electrons from water. It also generates a *pmf* across the thylakoid membrane composed of a proton gradient (ΔpH) and electrical gradient ($\Delta\Psi$); the *pmf* is used by the ATPase to generate ATP (proton translocation is shown in red dashed lines; ATP fluxes are shown in red plain lines). CEF (light pink solid arrow) and PCEF (magenta solid arrow) both contribute to the generation of the *pmf* but do not produce reducing equivalents since the e^- used for PCEF reduces O_2 to water. CMEF (pink solid arrow) encompasses multiple metabolic pathways by which reductants generated in the chloroplast are shuttled to the mitochondria and converted into ATP by the mitochondrial electron transport chain. NADPH and ATP generated by these different pathways are eventually used for transforming CO_2 into biomass, which reflects net photosynthesis. AOX, alternative oxidase; CBB, Calvin–Benson–Bassham; FDX, ferredoxin; FLVs, flavodiiron proteins; FNR, ferredoxin-$NADP^+$ reductase; Myxo, myxothiazol; PS, photosystem; PGR5/L1, PROTON GRADIENT REGULATION 5/like-1; SHAM, salicylhydroxamic acid; I, III, IV, respiratory complexes I, III, and IV.

CEF, PCEF, and CMEF each have the potential to sustain most net photosynthesis

While CMEF can power all net photosynthesis, the potential of CEF, PCEF, and the two subpathways of CMEF to energize net

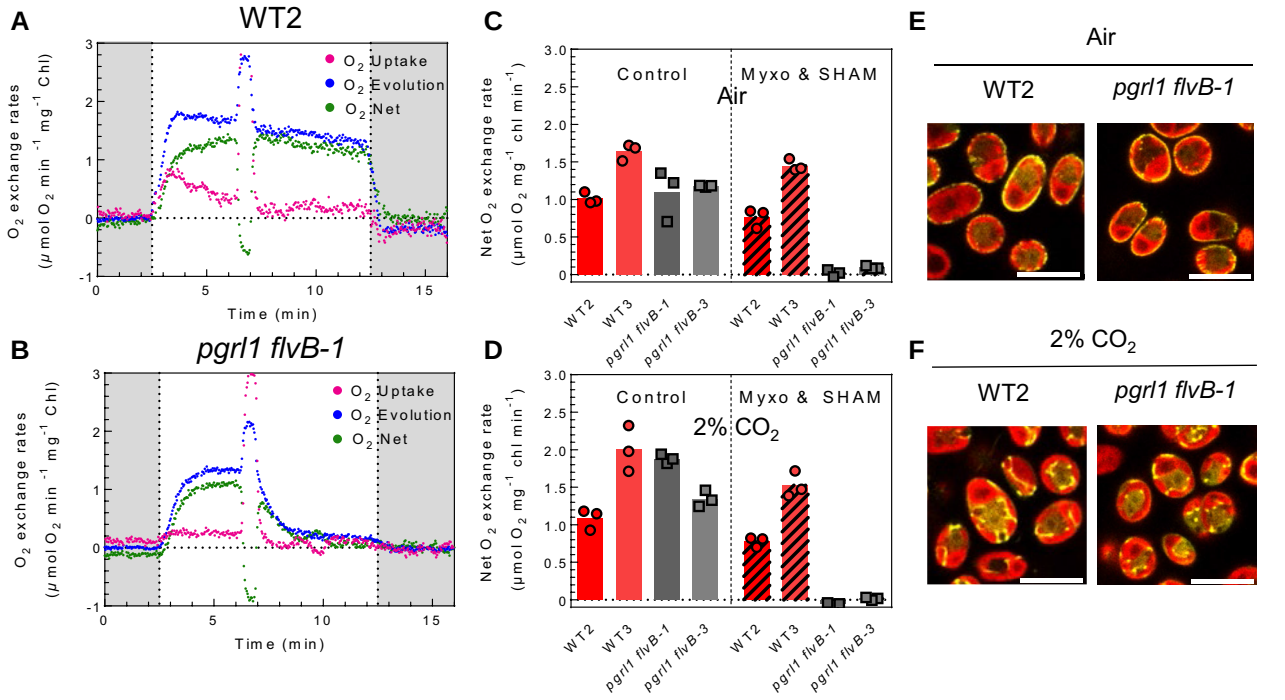

Figure 2. Dependence of net photosynthesis on CEF, PCEF, and CMEF. **A, B)** O_2 exchange rates upon a dark-to-light transition in WT2 **A)** and *pgrl1 flvB-1* **B)**. At $t = 6$ min, mitochondrial respiration inhibitors Myxo (2.5 μM) and SHAM (400 μM) were added to the reaction. Shown are representative traces of $n = 3$ biologically independent samples. **C, D)** Net O_2 evolution in *pgrl1 flvB-1* and *pgrl1 flvB-3* and their control strains (WT2 and WT3) in the absence (control) or presence (Myxo and SHAM) of Myxo (2.5 μM) and SHAM (400 μM) in cells grown in air **C)** or in 2% CO_2-enriched air **D)**. Values are taken after 9 min of illumination upon a dark to light transitions and normalized per chlorophyll content (chl). Bars show the average and dots show individual replicates ($n = 3$ biologically independent samples). Typical experiments used to extract these data are shown in Supplementary Fig. S2. **E, F)** Cross section images showing subcellular localization of mitochondrion-localized Clover (yellow fluorescence) in *pgrl1 flvB-1* and a control strain (WT2), grown in air **E)** or 2% CO_2-enriched air **F)**. Images are representative of 2 independent experiments. Scale bar: 10 μm. Clover/chlorophyll merged signals are shown. Images are representative of 2 experiments. Scale bar: 10 μm.

photosynthesis remains unclear. We sought to estimate it by measuring the effect of mitochondrial inhibitors on photosynthesis rates in single and double *pgrl1* and *flvB* mutants (Fig. 3, A to D). Inhibition of respiration decreased net photosynthesis by 40% to 50% in both the *flvB* and *pgrl1* single mutants (Fig. 3, A and B; Supplementary Figs. S1A and S2), showing that both CEF and PCEF, independently, have the potential to energize 50% to 60% of V_{Max} (Fig. 3E; Supplementary Fig. S1, A and B). Inhibition of respiration decreased the V_{Max} of all control strains by 10% to 20% (Supplementary Fig. S1A, S2, and S3) showing that combined activities of CEF and PCEF can power approximately 85% of photosynthesis (Fig. 3E). Based on the effects of SHAM or Myxo individually, on V_{Max} in *pgrl1 flvB* mutants (Fig. 3, C to E; Supplementary Figs. S1A and S2), we conclude that while the complex III and IV pathway of CMEF (Fig. 1) can power most net photosynthesis on its own (Fig. 3D), the AOX pathway (Fig. 1) can only sustain approximately 45% of V_{Max} (Fig. 3E). Because the amount of the terminal oxidases involved in CMEF does not differ in the *pgrl1 flvB* mutants and their control strains (Supplementary Fig. S6), these values likely reflect WT capacities. We also quantified net photosynthesis based on inorganic carbon (C_i) uptake (Supplementary Figs. S7 and S8). For all strains tested, the inhibitory effects on V_{max} measured as net C_i uptake were similar to that observed on net O_2 production (Supplementary Fig. S7). We conclude from these experiments that CEF, PCEF, and CMEF can sustain photosynthetic C_i uptake on their own but that only the complex III and IV pathway of CMEF is efficient enough to reach near-maximal photosynthesis levels.

CEF, PCEF, and CMEF show different efficiencies in sustaining net photosynthesis

The strong capacity of CMEF to power photosynthesis at its maximal rate by using less than 10% of additional electron flow relative to net photosynthesis (*%-LEF*) was surprising. This contrasts with around 30%-*LEF* of PCEF not being sufficient to reach maximal photosynthesis (Supplementary Fig. S3). We hypothesized that this difference could result from differences in the efficiencies of the alternative pathways to power net photosynthesis. Indeed, mechanistically, for each electron flowing once through the different pathways (CEF, PCEF, the AOX, or the complex III and IV pathways of CMEF), the total number of protons translocated across the thylakoid and/or the inner mitochondrial membranes highly differs (Burlacot 2023). To experimentally quantify the efficiency of the different pathways in energizing net photosynthesis, we introduce a metric, the net electron (e^-) yield of a pathway defined by the following equation:

$$\text{net } e^- \text{ yield} = \frac{e^-(\text{net photosynthesis})}{e^-(\text{net photosynthesis}) + e^-(\text{alternative pathway})},$$

where e^- (net photosynthesis) is the flux of photosynthetic electrons directly used for net photosynthesis and e^- (alternative pathway) is the flux of photosynthetic electrons through a given alternative pathway under conditions where only this alternative pathway is active (in addition to LEF). Therefore, the net e^- yield of an alternative pathway, which is determined when only that specific alternative pathway is operating, characterizes

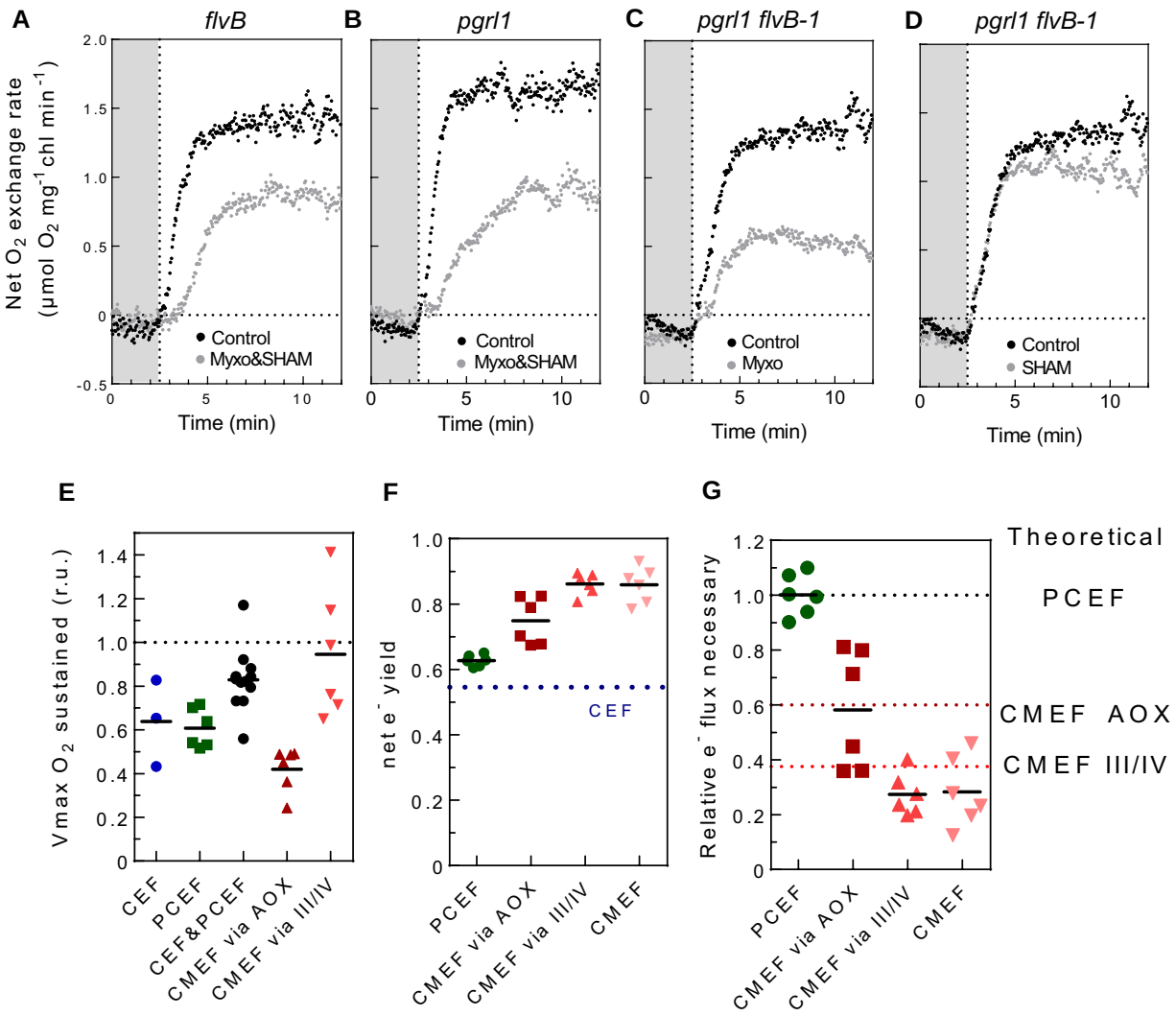

Figure 3. Relative efficiencies of CEF, PCEF, and CMEF in energizing net photosynthesis. **A to D)** Net O_2 evolution measured during a dark to light transition in *flvB* **A)**, *pgrl1* **B)**, *pgrl1 flvB*-2 **C, D)**, treated (gray dots) or not treated (black dots) with both Myxo (2.5 µM) and SHAM (400 µM) **A, B)** or with only one inhibitor **C, D)**. Shown are representative traces of 3 biological replicates. **E)** Relative V_{max} measured when a given set of alternative electron pathways are active after treatment with Myxo (2.5 µM), SHAM (400 µM), or both inhibitors; CEF (blue, *flvB* treated with Myxo and SHAM), PCEF (green, *pgrl1* treated with Myxo and SHAM), CEF&PCEF (dark, control strains treated with Myxo and SHAM), CMEF via AOX (burgundy, *pgrl1 flvB* treated with Myxo), and CMEF via III/IV (red, *pgrl1 flvB* treated with SHAM). **F)** Net electron yield of PCEF (green), CMEF via AOX (purple), CMEF via III/IV (red), CMEF (pink), and CEF (dotted line). Similar net electron yields were also determined for PCEF in 2% CO_2-grown cells and a slightly lower net electron yield for CMEF (Supplementary Fig. S9D). **G)** Electron flux relative to PCEF required to power similar levels of net photosynthesis when relying on a single pathway. Data shown are individual extrapolations based on measured net electron yields. In **E)**, **F)**, and **G)**, bars show the average and dots show individual replicates ($n \geq 3$ biologically independent samples).

the efficiency of electrons passing through it in powering net photosynthesis under a given physiological condition. Note that the net e^- yield, thus, does not reflect the rate or the importance of the pathway considered but rather its capacity to translocate H^+ for each electron.

We used this equation and experiments from Fig. 3, A to E to quantify the net e^- yield of each pathway (Fig. 3F; Supplementary Fig. S9). The net e^- yield of PCEF was estimated at 0.65, whereas that of CMEF at 0.85 (Fig. 3F), indicating a better efficiency of CMEF in driving CO_2 fixation relative to PCEF. In the absence of an established method to quantifying CEF in physiologically relevant conditions (Burlacot et al. 2022), CEF net e^- yield was estimated to be around 0.55 by hypothesizing that an electron passing once through CEF is 1.5 times less efficient at generating a *pmf* than if it would pass through PCEF (Kramer and Evans 2011; Burlacot 2023) (see Materials and Methods). In the case of CMEF, the net e^- yield of the AOX pathway was lower than that of the complex III and IV pathway (Fig. 3F), likely reflecting the proton translocating capacity of each pathway (Fig. 1) (Burlacot 2023). Using the net e^- yields of each pathway, we then compared the flux of electrons required to power the same amount of net photosynthesis relative to PCEF (Fig. 3G). Strikingly, theoretical values were in accord with values experimentally determined by the net e^- yields (Fig. 3G). Suggesting that under our conditions, the measured differences of efficiencies to power net photosynthesis were due to their mechanistic H^+/e^- transfer capacity. We conclude from these experiments that CMEF pathways are more efficient than PCEF and CEF at energizing CO_2 fixation and that this difference arises from its higher H^+/e^- transfer capacity, which likely leads to a higher capacity to generate ATP.

Estimating the respective contributions of CEF, PCEF, and CMEF during steady-state photosynthesis and growth

A key remaining question is to determine which set of pathways is active in vivo when all are functional and to what extent each of them contributes to net photosynthesis under physiological conditions. We thus sought to estimate (i) the relative electron flux via each pathway and (ii) their contribution to energize net photosynthesis during steady-state photosynthesis. We used two different approaches, one based on the effect of mutations and the other based on the effect of respiratory inhibitors. As both approaches are based on pathway inhibition, they are potentially biased by the high level of redundancy existing between them and the existence of compensatory mechanisms (Cardol et al. 2009; Dang et al. 2014; Burlacot et al. 2022). However, the two approaches differ in the way compensatory mechanisms contribute, with mutants being more subject to compensation than the short-term effects of inhibitors. In the mutant-based approach, PCEF was quantified by subtracting O_2 uptake rates in the *flvB* mutant from its control parental strain (allowing the calculation of $PCEF_{mut}$ and $CMEF_{mut}$) (Supplementary Fig. S10). In the inhibitor-based approach, CMEF was quantified by subtracting O_2 uptake rates between SHAM plus Myxo treated and untreated control strains (allowing the calculation of $PCEF_{inhib}$ and $CMEF_{inhib}$) (Supplementary Fig. S10).

The two methods differ somewhat in their estimates of PCEF and CMEF (Fig. 4, A and B; Supplementary Fig. S11), with a higher CMEF contribution being estimated using the mutant method. On average, PCEF and CMEF represent a flux of between 10% to 20%-*LEF* and 5% to 10%-*LEF*, respectively (Fig. 4A). Based on the respective net e^- yield of each pathway, we can estimate that 10% to 30% and 30% to 60% of CO_2 fixation is sustained by PCEF and CMEF, respectively (Fig. 4B). Since CEF sustains the remaining net photosynthesis, we estimated that 25% to 30% of CO_2 fixation is powered by CEF (Fig. 4B), which corresponds to a CEF of about 25%-*LEF* assuming a net e^- yield of CEF of 0.55 (Fig. 4A). We also tried to use mutants impaired in the NADH DEHYDROGENASE 4 subunit of respiratory complex I (*nd4*), PGRL1, or both (*nd4 pgrl1*) (Larosa et al. 2018) as a third method for estimating respective contributions of the different pathways (Supplementary Fig. S12). However, the low inhibition of respiration rates in *nd4* and *nd4 pgrl1* mutants, indicating the existence of complex I-independent respiration pathways (Supplementary Fig. S12A) makes these mutants unsuitable for this purpose.

To further assess the contribution of CEF, PCEF, and CMEF over the long term, growth tests were performed on the different strains in the absence or presence of the respiration inhibitor Myxo. While Myxo has no effect on the growth of control strains and single *flvB* or *pgrl1* mutants in moderate light intensities (Fig. 4C), growth of *pgrl1 flvB* was impaired in the presence of the inhibitor (Fig. 4C; Supplementary Fig. S13, B and C). Interestingly, at low light intensity (30 μmol photons m^{-2} s^{-1}), the effect of Myxo on the double mutant was absent (Supplementary Fig. S13A), suggesting that the AOX pathway of CMEF has the potential to fully power net photosynthesis in low light conditions. Therefore, whereas CEF, PCEF, and CMEF all contribute to energizing photosynthesis, CMEF, although representing a relatively small flux, has the potential to fuel CO_2 fixation and biomass accumulation thanks to its high capacity for H^+ translocation per e^-.

Discussion

Since the first description of CEF by Arnon (1959), the question was raised as to whether LEF could sustain the ATP requirement of photosynthetic CO_2 fixation (Arnon 1959), and it was proposed that photosynthetic electron flows, other than LEF, are involved in balancing the ATP/NADPH ratio to sustain CBB cycle function (Arnon 1959; Allen 2003) and other metabolic processes. Since then, several mechanisms of CEF, PCEF, and CMEF have been uncovered (Munekage et al. 2002, 2004; Helman et al. 2003; Tomaz et al. 2010) as well as some compensations among those different mechanisms (Cardol et al. 2009; Petroutsos et al. 2009; Dang et al. 2014; Storti et al. 2019; Storti et al. 2020; Burlacot et al. 2022), but the importance and relative efficiency of each mechanism remain mostly unknown. Here, we have shown that in *Chlamydomonas* PGRL1-controlled CEF, FLV-mediated PCEF, and both the AOX and complex III/IV/cytochrome oxidase pathways of CMEF can all supply additional energy to complement LEF for CO_2 fixation. The net e^- yields of CEF, PCEF, and CMEF greatly differ; CMEF is the most electron efficient and contributes importantly to the extra ATP requirements of CO_2 fixation in continuous, saturating light. Note that in spite of the ongoing controversy of how PGRL1 is involved in CEF (Nawrocki et al. 2019), a clear integration is observed among PGRL1-controlled CEF, PCEF, and CMEF, with these different pathways able to compensate for a reduction in the activities of the other pathways. Importantly, we observed similar effects on net O_2 and CO_2 exchange (Supplementary Fig. S7), thus showing that all effects measured on net photosynthesis correspond to changes in CO_2 fixation and eventually biomass production and growth (Fig. 4 C).

Some compensation between CEF, PCEF, and CMEF has been previously reported; a *Chlamydomonas* PGRL1-deficient strain exhibits increased CMEF and PCEF (Dang et al. 2014) and mutants of complexes I and III show enhanced rates of CEF (Cardol et al. 2009). We observed an elevated CMEF in the absence of FLV (Fig. 4, A and B) with a higher level of terminal oxidases associated with CMEF (Supplementary Fig. S6), corroborating cross-compensation among the three mechanisms of alternative electron flow. In diatoms, while CMEF is considered to be a major driver of CO_2 fixation, inhibition of CMEF only leads to a ~20% decrease of the PSII yield (Bailleul et al. 2015), which might also reflect compensation by CEF. We also conclude, based on the fact that no CO_2 fixation could be detected in the double *pgrl1 flvB* mutants treated with inhibitors of mitochondrial respiration, that neither the NDA2-mediated CEF nor O_2 reduction mediated by the plastid terminal oxidase or Mehler reactions has the potential by themselves to sustain a measurable amount of net photosynthesis, which is in agreement with previous studies concluding that these pathways represent a small fraction of alternative electron flow (Alric et al. 2010; Houille-Vernes et al. 2011; Nawrocki et al. 2019) (Fig. 2 B).

Establishing the quantitative contribution of each pathway in the WT strain in the absence of perturbation of any alternative pathway is a challenging task to which the approaches we have developed here provide an imperfect answer. Indeed, the proposed quantification of each pathway relies on the assumption that inhibiting one pathway (CMEF or PCEF) does not impact the flow through the others, an assumption not likely to be accurate since compensation among the different pathways has been previously documented (Cardol et al. 2009; Dang et al. 2014; Burlacot et al. 2022). Therefore, our approach attempts to evaluate the respective contributions of each pathway until an integrative quantification method is available. Here, the mutant method likely overestimates CMEF and the inhibitor method likely overestimates PCEF; both approaches likely overestimate CEF. It is clear, however, that no single pathway sustains net photosynthesis by itself (Supplementary Fig. S11B), which might reflect a rather

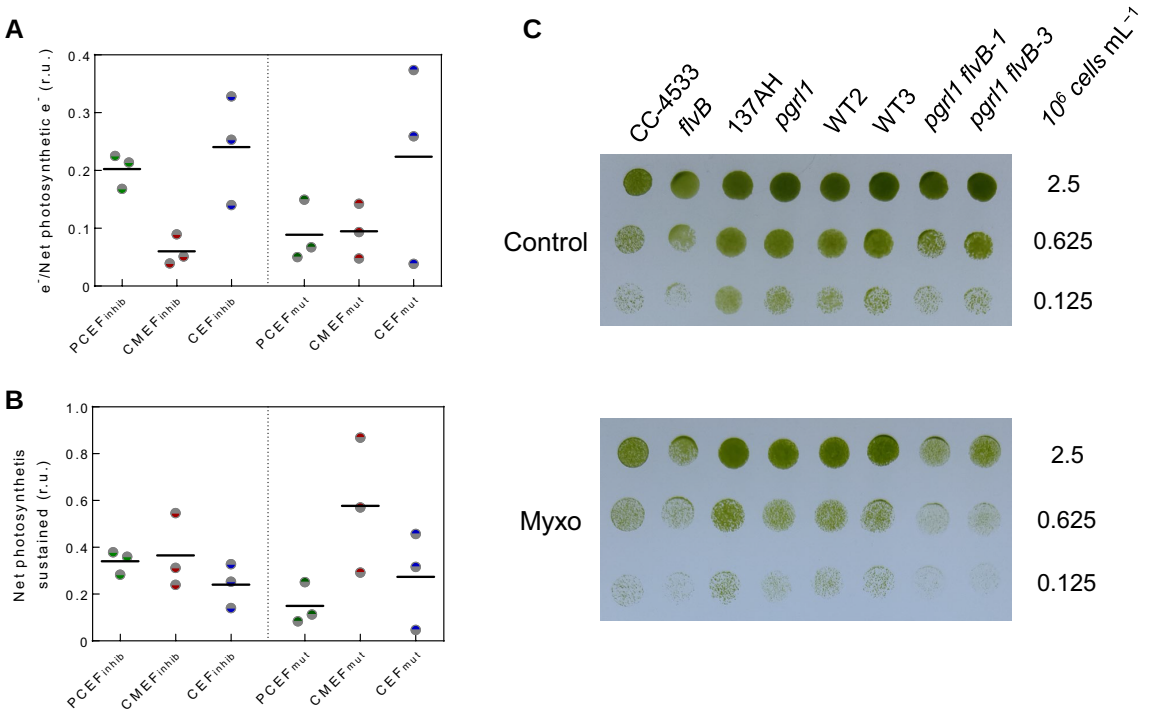

Figure 4. Contribution of CEF, PCEF, and CMEF to the electron flow, net photosynthesis, and growth. **A)** Electron flow through PCEF, CEF, and CMEF relative to LEF was determined in the WT strain CC-4533 by 2 different methods, one based on the use of inhibitors (inhib) and the other on mutants (mut). Data used for these calculations are the same as for Fig. 2C and Supplementary Fig. S2. **B)** Proportion of net photosynthesis powered by each electron flow (PCEF, CEF, and CMEF) in the control strain CC-4533 as measured by the inhibition (inhib) or mutant (mut) method. CC-4533 was chosen because it is the control strain for *flvB* and is therefore the only strain where both methods could be used. Data used for these calculations are the same as for **A)**. In **A)** and **B)**, bars show the average and dots show individual replicates ($n = 3$ biologically independent samples). **C)** Growth tests for *flvB* and *pgrl1* mutants, their corresponding control strains (CC-4533 and 137AH, respectively) and double mutants (*pgrl1 flvB-1* and *pgrl1 flv-3*) and their corresponding control strains (WT2 and 3). Cells were spotted on plates containing minimal medium at pH 7.2 and grown under continuous illumination (60 μmol photon m^{-2} s^{-1}) in the absence (upper panel) or presence (lower panel) of 2.5 μM Myxo in air enriched at 2% CO_2. Spots shown are representative of 10 independent experiments.

balanced contribution of the different pathways to CO_2 fixation in the WT. It is also noteworthy that, although concordant quantifications are seen in the different WT strains used, there is some level of variability (Supplementary Fig. S11), which might reflect the effect of the genetic background. In any case, it seems highly likely that, considering the high redundancy of alternative electron pathways of photosynthesis and the ability of each of them to sustain CO_2 fixation at a high rate, a dynamic mix of the different pathways may enable cells to better cope with variable environmental conditions (Burlacot 2023).

The net e^- yield, a tool to evaluate the efficiency of electron transport pathways

In support to LEF, the combined energetic outputs of PGRL1-controlled CEF and PCEF cannot sustain more than 80% of maximal CO_2 fixation (Fig. 3E) whereas the flux of e^- through each of these pathways individually can help sustain 60% of it (Fig. 3F). This suggests the existence of an intrinsic limitation of the flow of electrons through the photosynthetic electron transport chain, which is likely due to a *pmf*-induced photosynthetic control occurring at the cytochrome b_6f level (Rumberg et al. 1968; Stiehl and Witt 1969; Johnson and Berry 2021; Malone et al. 2021), an elevated *pmf* eliciting a block in electron flow across the b_6f complex. Engaging an electron pathway with a high net e^- yield, such as CMEF, might be a way to avoid this limitation since fewer electrons would be needed to power the same level of CO_2 fixation. Such a strategy seems to be used by diatoms (Bailleul et al. 2015), which lack FLVs and mosses, whose photosynthetic activity is impaired by inactivation of the mitochondrial respiratory complex I (Mellon et al. 2021).

Throughout the green lineage, the nature and activity of alternative electron flows are quite different. For example, angiosperms lack FLV-dependent PCEF (Peltier et al. 2010), harbor a NDH-1-dependent CEF pathway (Peltier et al. 2016), and have a weakly active CMEF (Raghavendra and Padmasree 2003). Since the NDH-1-dependent CEF translocates $4H^+/e^-$ (Strand et al. 2017), its net e^- yield is probably close to that of CMEF, strongly suggesting that in angiosperms, the NDH-1 complex can compensate when CMEF capacity is diminished. The latter is illustrated by the poor growth of *Arabidopsis* (*Arabidopsis thaliana*) mutants impaired in both CEF pathways (PGR and NDH-1) (Munekage et al. 2004). Because of the number of key proteins and biochemical reactions involved in CMEF, its high net e^- yield may not be as rapidly accessible as CEF or PCEF during environmental fluctuations. While, under light-limiting conditions, a high net e^- yield pathway might be advantageous, a less efficient pathway would contribute to the safe dissipation of excess absorbed light energy and diminished reactive oxygen production at saturating light intensities. Overall, it remains to be determined to what extent harboring a palette of alternative electron flows with varying yields and likely different time responses is critical for sustaining photosynthetic performance under dynamic, natural conditions.

Note here that while modulation of the capacity of membranes to transform *pmf* into ATP may modulate the absolute net e^- yield of each pathway, the relative net e^- yield of CEF and PCEF would not change if they are embedded in the same thylakoid system.

Similarly, even under conditions in which the mitochondrial respiration would be partially or fully uncoupled, the net e^- yield of CMEF would be at least as good as PCEF due to the generation of a *pmf* across the thylakoid membranes (Burlacot 2023). Hence, if CEF, PCEF, and CMEF are all competing for the same photosynthetic electrons, electrons passing through CMEF and PCEF should always be more efficient than CEF in powering net photosynthesis. Measuring a relative positioning of the net e^- yield of each pathway that is different than the one described here would be an indication of spatially separated electron transport chains dedicated to specific pathways in vivo.

Additional energy cost of photosynthesis

Allen (2002) previously estimated that a PCEF representing only 16%-*LEF* would be sufficient, in addition to LEF, to satisfy the ATP and NADPH requirement of the CBB cycle. Our conclusions are strikingly different since we estimate that if only PCEF was active, it would have to represent 54%-*LEF* to sustain CO_2 fixation. This discrepancy reflects the actual metabolic cost of CO_2 fixation that exceeds the ATP and/or H^+ requirement of the CBB cycle due to other processes that depend on proton gradient energization such as protein synthesis and transporter activities or to the presence of proton leakages through energized membranes. In addition to extra ATP/H^+ requirements, our measurements reveal that for each CO_2 molecule fixed, around two molecules of O_2 are generated (Supplementary Figs. S7 and S8), suggesting that half of the net reductant generated is used in metabolic processes other than the CBB cycle. It is worth noting here that similar conclusions have recently been reached in two marine diatoms (Shimakawa and Matsuda 2024) and in angiosperms where reductant and carbon fluxes are heavily channeled toward central carbon metabolism (Treves et al. 2022). Finally, in natural environments, either terrestrial or aquatic, CO_2 fixation is further limited by the concentration of atmospheric CO_2, which can trigger photorespiration in C_3 plants or induction of the CCM in C_4 plants and algae. All these mechanisms would require additional energy for their activities (Osmond 1981; Takabayashi et al. 2005; Walker et al. 2014; Burlacot et al. 2022), making alternative electron pathways of photosynthesis even more critical for sustaining plant and algal CO_2 capture. Given the strong capacity of CMEF to sustain photosynthesis and its high H^+/e^- conversion capacity, it is timely to reevaluate its importance during photosynthesis across photosynthetic eukaryotes.

Materials and methods

Strains and growing conditions

C. reinhardtii flvB and *pgrl1* single mutants and their respective parental strains CC-4533 (for *flvB*) and 137AH (for *pgrl1*) were previously described (Tolleter et al. 2011; Chaux et al. 2017). *flvB pgrl1*–1, -2, and -3 double mutant and their respective sibling strains WT2 and WT3 (used here as control strains) have been described previously (Burlacot et al. 2022) and are all from the progeny of a crossing of *flvB* and *pgrl1* performed in Burlacot et al. (2022). Because *pgrl1 flvB* double mutants were obtained by crossing the two single mutants that have different genetic backgrounds (as described in Burlacot et al. 2022), the control strains used are siblings that resulted from the cross and that contained WT copies and levels of the FLVB and PGRL1 proteins. *pgrl1-2* is a mutant impaired in accumulation of the PGRL1 protein originating from crossing *flvB* and *pgrl1* performed in Burlacot et al. (2022). Complex I-deficient strains and the *pgrl1* mutant used in Supplementary Fig. S12 have been described in Larosa et al. (2018). All strains were grown photoautotrophically in 125-mL flasks with cotton stoppers at 25°C in a buffered minimal medium (20 mM MOPS pH 7.2) under constant illumination (80 μmol photons m^{-2} s^{-1}) either under ambient CO_2 or 2% CO_2 in air. Among *pgrl1 flvB* double mutants and their control strains already described (Burlacot et al. 2022), *pgrl1 flvB-1* and *pgrl1 flvB-3* and WT2 and 3, respectively, were used for physiological measurements since their maximal photosynthesis was representative of other double mutants and control strains (Burlacot et al. 2022). All strains used in this study apart from the ones in Supplementary Fig. S12 are available under the same names used here (except for *flvB*, which is available as *flvB-21*) at the Chlamydomonas Resource Center (www.chlamycollection.org). The spectrum of the growing light used is shown in Supplementary Fig. S14. Throughout the manuscript, a "biologically independent experiment" refers to a replication that has been done with a fresh new liquid culture of the strains described, seeded from the source plates.

Gas exchange measurements

Gas exchange rates were measured using MIMS. Cells grown in air enriched or not at 2% CO_2 were collected during the exponential phase by centrifugation at 450 × *g* for 3 min and resuspended in 1.5 mL of fresh buffered minimal medium (pH 7.2) at 30 μg chlorophyll mL^{-1}. HCO_3^- was subsequently added to the cell suspension (10 mM final concentration). The cell suspension was then placed in the MIMS reaction vessel (mounted with a 1 mil Teflon membrane), 2 mL of ^{18}O-enriched O_2 (97% ^{18}O Eurisop, France) was bubbled in the suspension. After closing the vessel, gas exchange was recorded during a dark-to-light transition (2,000 μmol photons m^{-2} s^{-1}; green LEDs picked at 525 nm; Luminus reference PT-121-G-L11-MPK). Light intensity was set to be saturating (Supplementary Fig. S15) using weakly absorbed green light for better homogeneity. Calculations of gross and net photosynthesis were done using the MIMS analysis software as previously described (Burlacot et al. 2020). In some experiments, SHAM (400 μM final concentration) and Myxo (2.5 μM final concentration) were added 1 min before the beginning of the measurements, except for the data presented in Fig. 2, A and B, where inhibitors were added during the measurement. Note here that SHAM has been reported to not inhibit the plastid terminal oxidase (Cournac et al. 2000). All net O_2, net CO_2, gross O_2 exchange, net e^- yield, e^- flow, and net photosynthesis sustained shown as histograms in Figs. 2 to 4 and Supplementary Figs. S1, S7, S9, and S11 are based on measurements after 9 min of illumination.

Clover expressing cells

137AH, WT2, *pgrl1*, *flvB*, and *pgrl1flvB-1* and -2 expressing the mitochondrion-targeted fluorophore Clover (mito-Clover) were generated as described in Harmon et al. (2022). Briefly, cells were transformed with a linearized plasmid encoding mito-Clover and a hygromycin resistance cassette using the Max Efficiency Reagent (Invitrogen). Clones resistant to hygromycin were screened for Clover fluorescence using a M1000 Tecan plate reader (excitation: 488/7 nm; emission: 515/10 nm) and mitochondrial signal was checked by confocal microscopy (described below). Selected clones were grown at 80 μmol photons m^{-2} s^{-1} in 25 mL minimal medium in 125-mL flasks, in the presence of either normal or 2% CO_2-enriched air until they reached a density of ~10 μg chlorophyll mL^{-1}. An aliquot of each culture was then briefly concentrated by centrifugation at 1,500 × *g*, and cells

were layered on an 18-well microscope slide. Images were acquired using a TCS SP8 confocal laser-scanning microscope (Leica) and a 63× objective. Acquisition settings were as follows: Clover excitation 488 nm, emission 500 to 547 nm; chlorophyll excitation 488 nm, and emission 694 to 733 nm. For homogeneity and clarity, signal intensities of each channel were adjusted using the Fiji software. Strains expressing mito-Clover used in this article are publicly available from the Chlamydomonas Resource Center (https://www.chlamycollection.org) under the following CC numbers: CC-6056 (137AH), CC-6059 (WT2), CC-6057 (*flvB*), CC-6058 (*pgrl1*), CC-6060 (*pgrl1 flvB-1*), and CC-6061 (*pgrl1 flvB-1*).

Growth tests

The different *Chlamydomonas* strains were cultivated at an air level of CO_2 under moderate light (80 µmol photons m^{-2} s^{-1}) at 25 °C. Cells were collected during exponential growth and diluted in fresh minimal medium to 0.125, 0.625, or 2.5 10^6 cells mL^{-1}. Seven-microliter drops were spotted on 2% Agar plates of minimal medium (buffered with 20 mM MOPS pH 7.2) with or without Myxo (2.5 µM final concentration) and exposed to air enriched with 2% CO_2. Homogeneous light was supplied by LED panels (see its spectrum in Supplementary Fig. S14B); the different light intensities were obtained with various neutral filters. Temperature was maintained at 25 °C at the level of plates by means of fans.

Net electron yield calculation

The net e^- yield of a given alternative electron pathway is defined as the proportion of electrons generated downstream PSI that are used for net photosynthesis when only this alternative electron pathway is active, following this equation:

$$\text{net}e^- \text{yield} = \frac{e^-(\text{net photosynthesis})}{e^-(\text{net photosynthesis}) + e^-(\text{alternative pathway})}, \quad (1)$$

where e^- (net photosynthesis) is the flux of photosynthetic electrons directly used as reductants for net photosynthesis and e^- (alternative pathway) is the flux of photosynthetic electrons through an alternative pathway. Because, for PCEF and CMEF, the sum of e^- (alternative pathway) and e^- (net photosynthesis) equals gross photosynthesis, net electron yields of PCEF and CMEF were quantified using gross and net O_2 evolution in mutants harboring: only PCEF (*pgrl1* and *pgrl1-2* mutants treated with Myxo and SHAM) or only the AOX or the complex III/IV pathway of CMEF (*pgrl1 flvB-1* and -3 mutants treated with Myxo or SHAM, respectively). The net electron yield was then calculated for each pathway using the following equation:

$$\text{net}\, e^- \text{ yield} = \frac{\text{net } O_2 \text{ evolution}}{\text{gross } O_2 \text{ evolution}}. \quad (2)$$

The theoretical net electron yield of CEF was calculated based on the assumption that CEF translocates 1.5 less protons per electron across the thylakoid membranes than PCEF (Kramer and Evans 2011; Burlacot 2023) and that this is the driving force leading to net photosynthesis energization. Note that this later assumption is well supported by the independent results from Fig. 3G showing that the relative net electron yield of CMEF pathways and PCEF corresponds to their relative capacity at translocating protons across membranes. Hence, for the same net photosynthesis powered, CEF should be 1.5 times higher than PCEF, and the net electron yields of CEF could be written as follows:

$$\text{net}e^- \text{yield (CEF)} = \frac{e^-(\text{net in } pgrl1 \text{ Myxo SHAM})}{e^-(\text{net in } pgrl1 \text{ Myxo SHAM}) + e^-(\text{PCEF}) \times 1.5}, \quad (3)$$

where e^- (net in *pgrl1* Myxo SHAM) is the net photosynthesis measured in the *pgrl1* mutant treated with Myxo and SHAM (hence having only PCEF active) and e^- (PCEF) is the O_2 uptake rate in the same strain and condition.

Based on Equation (1), we can rewrite e^- (PCEF) as follows:

$$e^-(\text{PCEF}) = \frac{(1 - \text{net}\, e^- \text{ yield(PCEF)})}{\text{net}\, e^- \text{ yield(PCEF)}} \times e^-(\text{net in } pgrl1 \text{ Myxo SHAM}) \quad (4)$$

Hence, combining Equations (3) and (4):

$$\text{net}\, e^- \text{ yield (CEF)} = \frac{\text{net}\, e^- \text{ yield (PCEF)}}{1.5 - \frac{\text{net}\, e^- \text{ yield (PCEF)}}{2}}. \quad (5)$$

The net electron yield of CEF shown in Fig. 3 is using Equation (5) with the average net electron yield of PCEF. Note that the quantification of the net e^- yield in *Chlamydomonas* assumes that removing two pathways (elimination of CEF and CMEF in the *pgrl1* mutant treated with inhibitors of respiration and CEF and PCEF in the *pgrl1 flvB* double mutants) makes CO_2 fixation dependent only on the third pathway. This dependency is supported by the finding that the *pgrl1 flvB* double mutant treated with inhibitors of respiration is unable to support any CO_2 fixation, which also support the hypothesis that the contribution of other pathways, such as the NDA2-dependent CEF, is marginal. Also note that by definition, the net electron yield of a pathway is independent of the maximal capacity of this pathway but rather reflects a per electron efficiency of the pathway in powering net photosynthesis under the physiological condition where it is assessed.

Calculation of electron flows via each pathway and their contribution to net photosynthesis in WT strains

The electron flow through PCEF and CMEF was deduced on WT strain using two independent methods based on measurements of gross O_2 uptake made in Supplementary Figs. S2 and S3. In the so-called "mutant" method, CMEF was quantified as being the gross O_2 uptake measured in the *flvB* mutant. Then, PCEF was quantified by subtracting the CMEF to the O_2 uptake of CC-4533 (Supplementary Fig. S10). This method was only used for CC-4533 since it is the only control strain for the *flvB* mutant. In the so-called "inhibitor" method, PCEF was quantified as being the gross O_2 uptake remaining in control strains treated with SHAM and Myxo. Then, CMEF was quantified by subtracting the PCEF to the O_2 uptake in the same untreated control strain (Supplementary Fig. S10). The calculated electron flows of PCEF and CMEF were then used for each strain to quantify the net photosynthesis powered by each of them following the equations derived from Equation (1):

$$\text{net photoynthesis (AEF)} = e^-(\text{AEF}) \times \frac{\text{net}\, e^- \text{ yield (AEF)}}{1 - \text{net}\, e^- \text{ yield (AEF)}},$$

where net photosynthesis (AEF) is the net photosynthesis sustained by a specific alternative electron flow, e^- (AEF) is the electron flow through this alternative electron flow, and net e^- yield (AEF) is the net electron yield of this alternative electron flow.

The total of net photosynthesis powered in a strain by PCEF and CMEF was then compared to the measured net photosynthesis in this same strain to quantify the "missing" net photosynthesis that had to be powered by CEF. Then, the electron flow through CEF

(e^- (CEF)) was calculated by the following equation derived from Equation (1):

$$e^-(\text{CEF}) = \text{missing net} \times \frac{1 - \text{net } e^- \text{ yield (CEF)}}{\text{net } e^- \text{ yield (CEF)}},$$

where missing net is the calculated net photosynthesis that is not powered by PCEF and CMEF and net e^- yield (CEF) is the net electron yield of CEF.

Protein extraction and immunodetection

Cells were harvested by centrifugation at 1,000 × *g* for 5 min. Total cellular protein was extracted by heating the cell pellet at 100°C for 1 min using an extraction aqueous solution composed of 1% (*v*/*v*) SDS, 100 mM DTT, 1 mM aminocaproic acid, and 1 mM benzamidine hydrochloride buffered with 60 mM Tris (pH 6.8). The resulting cell lysate was then centrifuged at 10,000 × *g* for 5 min to obtain the supernatant. The supernatant was subsequently incubated with acetone (80% -v/v- final concentration) at −20°C for 1 h. The protein pellet was collected by centrifugation at 5,000 × *g* for 5 min and stored in aqueous solution containing 1% (*v*/*v*) SDS and 5 mM DTT and buffered with 60 mM Tris (pH 6.8). Protein content was estimated (Microplate BCA Protein Assay Kit-reducing agent compatible, Thermo Scientific) with bovine serum albumin as the standard. Protein extracts (10 μg protein) were loaded on a 12% SDS–PAGE gel and run for 1 h at 150 V in Tris-glycine SDS buffer and transferred onto a nitrocellulose membrane using semi-dry transfer (Trans-Blot Turbo, Bio-Rad). Immunoblot detection was performed using antibodies raised against FlvB (1:1,000) (Chaux et al. 2017) and Pgrl1 (1:5,000) (Tolleter et al. 2011). Other antibodies against AOX1 (1:10,000) (AS06 152) and COXIIB (1:10,000) (AS06 151) were obtained from Agrisera (https://www.agrisera.com/). An anti-rabbit HRP-conjugated antibody (1:50,000) (AS09 602, Agrisera) was used as a secondary antibody for immunodetection. Precision Plus Protein Dual Color Standards (Bio-Rad) was used as the molecular weight marker. Uncropped and unprocessed scans of the blots shown in this study are visible in Supplementary Fig. S16.

Accession numbers

Genes studied in this article can be found on https://phytozome-next.jgi.doe.gov/ under the loci Cre12.g531900 (*FLVA*), Cre16.g691800 (*FLVB*), Cre07.g340200 (*PGRL1*), Cre09.g395950 (*AOX1*), Cre03.g169550 (*AOX2*), and Cre01.g049500 (*COXIIB*).

Acknowledgments

The authors acknowledge the constructive comments on the manuscript from Dr. Joe Berry, Dr. Jennifer Johnson, Evan Saldivar, and Leron Perez, technical support from Michel Philibert and Emmanuel Capra, and editing help by Dr. Solène Moulin. We thank Professor Claire Remacle for providing us with complex I-deficient strains. We would like to thank the Carnegie Advanced Imaging Facility for the use of microscopy instruments (Leica TCS SP8 confocal laser-scanning microscope).

Author contributions

A.B. led and coordinated the research; A.B. and G.P. designed the research; A.B., C.S., J.F., O.D., S.M., V.E., A.M., and G.P. performed the research; A.B. and G.P. contributed new reagents/analytic tools; A.B. analyzed the data and made all figures; and A.B. and G.P. wrote the paper with inputs from Y. L.-B. and A.G.

Supplementary data

The following materials are available in the online version of this article.

Supplementary Figure S1. Effect of mitochondrial inhibitors on O_2 exchange rates on mutants and control strains grown at air level of CO_2.

Supplementary Figure S2. O_2 exchange rates in *pgrl1 flvB* double mutants and their control strains grown at air level of CO_2.

Supplementary Figure S3. O_2 exchange rates in *pgrl1* and *flvB* single mutants and their control strains grown at air level of CO_2.

Supplementary Figure S4. O_2 exchange rates in *pgrl1*, *pgrl1 flvB*, and their control strains grown in air enriched with 2% CO_2.

Supplementary Figure S5. Localization of mitochondria in *pgrl1*, *flvB*, *pgrl1 flvB*-1 and -2, and their control strain in air enriched or not with 2% CO_2.

Supplementary Figure S6. Immunodetection of proteins involved in CMEF, PCEF, and CEF in the strains used in this study

Supplementary Figure S7. Comparison of net inorganic carbon fixation and net O_2 production.

Supplementary Figure S8. Net Ci and O_2 exchange rated in *pgrl1* and *flvB* single and double mutants and the control strains WT2 and WT3.

Supplementary Figure S9. Net O_2 exchange rates characteristic and e^- quantum yield measured in strains grown in air enriched with 2% CO_2.

Supplementary Figure S10. Illustration of the method used to quantify the contribution of each photosynthetic electron flow to CO_2 fixation.

Supplementary Figure S11. Quantification of the contribution of each photosynthetic electron flow to net photosynthesis.

Supplementary Figure S12. Net O_2 exchange rates characteristic of mutants impaired in respiratory complex I and PGRL1.

Supplementary Figure S13. Growth of mutant and control strains at various light intensities.

Supplementary Figure S14. Growing light spectra.

Supplementary Figure S15. Light saturation curve of net O_2 exchange rate measured with green actinic light.

Supplementary Figure S16. Original images of immunoblots against the AOX1 and the respiratory cytochrome oxidase (CoxIIB) shown in Supplementary Fig. S6.

Supplementary Figure S17. Original images of immunoblots against FLVB and PGRL1 shown in Supplementary Fig. S6.

Funding

This work was supported by the Carnegie Institution for Science (A.B. and A.G.) and the ANR grants OTOLHYD n° ANR-18-CE05-0029 (G.P.) and AlgalCCM n°ANR-22-CE44-0023-01 (G.P., A.M., and V.E.). This work was also in part supported by DOE award DE-SC0019417 (A.G. and A.B.).

Conflict of interest statement. None declared.

Data availability

All data needed to evaluate the conclusions in the paper are present in the paper and/or the Supplemental material.

References

Alboresi A, Storti M, Morosinotto T. Balancing protection and efficiency in the regulation of photosynthetic electron transport

across plant evolution. *New Phytol*. 2019:221(1):105–109. https://doi.org/10.1111/nph.15372

Allahverdiyeva Y, Mustila H, Ermakova M, Bersanini L, Richaud P, Ajlani G, Battchikova N, Cournac L, Aro EM. Flavodiiron proteins Flv1 and Flv3 enable cyanobacterial growth and photosynthesis under fluctuating light. *Proc Natl Acad Sci U S A*. 2013:110(10):4111–4116. https://doi.org/10.1073/pnas.1221194110

Allen JF. Photosynthesis of ATP—electrons, proton pumps, rotors, and poise. *Cell*. 2002:110(3):273–276. https://doi.org/10.1016/S0092-8674(02)00870-X

Allen JF. Cyclic, pseudocyclic and noncyclic photophosphorylation: new links in the chain. *Trends Plant Sci*. 2003:8(1):15–19. https://doi.org/10.1016/s1360-1385(02)00006-7

Alric J, Johnson X. Alternative electron transport pathways in photosynthesis: a confluence of regulation. *Curr Opin Plant Biol*. 2017:37:78–86. https://doi.org/10.1016/j.pbi.2017.03.014

Alric J, Lavergne J, Rappaport F. Redox and ATP control of photosynthetic cyclic electron flow in *Chlamydomonas reinhardtii* (I) aerobic conditions. *Biochim Biophys Acta*. 2010:1797(1):44–51. https://doi.org/10.1016/j.bbabio.2009.07.009

Arnon DI. Conversion of light into chemical energy in photosynthesis. *Nature*. 1959:184(4679):10–21. https://doi.org/10.1038/184010a0

Arnon DI. The discovery of photosynthetic phosphorylation. *Trends Plant Sci*. 1984:9(6):258–262. https://doi.org/10.1016/0968-0004(84)90159-2

Bailleul B, Berne N, Murik O, Petroutsos D, Prihoda J, Tanaka A, Villanova V, Bligny R, Flori S, Falconet D, et al. Energetic coupling between plastids and mitochondria drives CO_2 assimilation in diatoms. *Nature*. 2015:524(7565):366–369. https://doi.org/10.1038/nature14599

Burlacot A. Quantifying the roles of algal photosynthetic electron pathways: a milestone towards photosynthetic robustness. *New Phytol*. 2023:240(6):2197–2203. https://doi.org/10.1111/nph.19328

Burlacot A, Burlacot F, Li-Beisson Y, Peltier G. Membrane inlet mass spectrometry: a powerful tool for algal research. *Front Plant Sci*. 2020:11:1302. https://doi.org/10.3389/fpls.2020.01302

Burlacot A, Dao O, Auroy P, Cuiné S, Li-Beisson Y, Peltier G. Alternative photosynthesis pathways drive the algal CO_2 concentrating mechanism. *Nature*. 2022:605(7909):366–371. https://doi.org/10.1038/s41586-022-04662-9

Burlacot A, Peltier G. Energy crosstalk between photosynthesis and the algal CCM. *Trends Plant Sci*. 2023:28(7):795–807. https://doi.org/10.1016/j.tplants.2023.03.018

Cardol P, Alric J, Girard-Bascou J, Franck F, Wollman FA, Finazzi G. Impaired respiration discloses the physiological significance of state transitions in *Chlamydomonas*. *Proc Natl Acad Sci U S A*. 2009:106(37):15979–15984. https://doi.org/10.1073/pnas.0908111106

Cardol P, Gloire G, Havaux M, Remacle C, Matagne R, Franck F. Photosynthesis and state transitions in mitochondrial mutants of *Chlamydomonas reinhardtii* affected in respiration. *Plant Physiol*. 2003:133(4):2010–2020. https://doi.org/10.1104/pp.103.028076

Chaux F, Burlacot A, Mekhalfi M, Auroy P, Blangy S, Richaud P, Peltier G. Flavodiiron proteins promote fast and transient O_2 photoreduction in *Chlamydomonas*. *Plant Physiol*. 2017:174(3):1825–1836. https://doi.org/10.1104/pp.17.00421

Cournac L, Redding K, Ravenel J, Rumeau D, Josse E-M, Kuntz M, Peltier G. Electron flow between photosystem II and oxygen in chloroplasts of photosystem I-deficient algae is mediated by a quinol oxidase involved in chlororespiration. *J Biol Chem*. 2000:275(23):17256–17262. https://doi.org/10.1074/jbc.M908732199

DalCorso G, Pesaresi P, Masiero S, Aseeva E, Nemann DS, Finazzi G, Joliot P, Barbato R, Leister D. A complex containing PGRL1 and PGR5 is involved in the switch between linear and cyclic electron flow in *Arabidopsis*. *Cell*. 2008:132(2):273–285. https://doi.org/10.1016/j.cell.2007.12.028

Dang KV, Plet J, Tolleter D, Jokel M, Cuine S, Carrier P, Auroy P, Richaud P, Johnson X, Alric J, et al. Combined increases in mitochondrial cooperation and oxygen photoreduction compensate for deficiency in cyclic electron flow in *Chlamydomonas reinhardtii*. *Plant Cell*. 2014:26(7):3036–3050. https://doi.org/10.1105/tpc.114.126375

Desplats C, Mus F, Cuine S, Billon E, Cournac L, Peltier G. Characterization of Nda2, a plastoquinone-reducing type II NAD(P)H dehydrogenase in *Chlamydomonas* chloroplasts. *J Biol Chem*. 2009:284(7):4148–4157. https://doi.org/10.1074/jbc.M804546200

Geraghty AM, Spalding MH. Molecular and structural changes in *Chlamydomonas* under limiting CO_2 (a possible mitochondrial role in adaptation). *Plant Physiol*. 1996:111(4):1339–1347. https://doi.org/10.1104/pp.111.4.1339

Gerotto C, Alboresi A, Meneghesso A, Jokel M, Suorsa M, Aro E-M, Morosinotto T. Flavodiiron proteins act as safety valve for electrons in *Physcomitrella patens*. *Proc Natl Acad Sci U S A*. 2016:113-(43):12322–12327. https://doi.org/10.1073/pnas.1606685113

Harmon J, Findinier J, Ishii NT, Herbig M, Isozaki A, Grossman A, Goda K. Intelligent image-activated sorting of *Chlamydomonas reinhardtii* by mitochondrial localization. *Cytometry A*. 2022:101-(12):1027–1034. https://doi.org/10.1002/cyto.a.24661

Helman Y, Tchernov D, Reinhold L, Shibata M, Ogawa T, Schwarz R, Ohad I, Kaplan A. Genes encoding a-type flavoproteins are essential for photoreduction of O_2 in cyanobacteria. *Curr Biol*. 2003:13(3):230–235. https://doi.org/10.1016/S0960-9822(03)00046-0

Houille-Vernes L, Rappaport F, Wollman F-A, Alric J, Johnson X. Plastid terminal oxidase 2 (PTOX2) is the major oxidase involved in chlororespiration in *Chlamydomonas*. *Proc Natl Acad Sci U S A*. 2011:108-(51):20820–20825. https://doi.org/10.1073/pnas.1110518109

Ilík P, Pavlovič A, Kouřil R, Alboresi A, Morosinotto T, Allahverdiyeva Y, Aro E-M, Yamamoto H, Shikanai T. Alternative electron transport mediated by flavodiiron proteins is operational in organisms from cyanobacteria up to gymnosperms. *New Phytol*. 2017:214(3):967–972. https://doi.org/10.1111/nph.14536

IPCC. *Climate change 2021: the physical science basis. Contribution of working group I to the sixth assessment report of the intergovernmental panel on climate change*. Cambridge, United Kingdom and New York, NY, USA: Cambridge University Press; 2021.

Jans F, Mignolet E, Houyoux PA, Cardol P, Ghysels B, Cuine S, Cournac L, Peltier G, Remacle C, Franck F. A type II NAD(P)H dehydrogenase mediates light-independent plastoquinone reduction in the chloroplast of *Chlamydomonas*. *Proc Natl Acad Sci U S A*. 2008:105-(51):20546–20551. https://doi.org/10.1073/pnas.0806896105

Joët T, Cournac L, Horvath EM, Medgyesy P, Peltier G. Increased sensitivity of photosynthesis to antimycin A induced by inactivation of the chloroplast ndhB gene. Evidence for a participation of the NADH-dehydrogenase complex to cyclic electron flow around photosystem I. *Plant Physiol*. 2001:125(4):1919–1929. https://doi.org/10.1104/pp.125.4.1919

Johnson X, Alric J. Central carbon metabolism and electron transport in *Chlamydomonas reinhardtii*: metabolic constraints for carbon partitioning between oil and starch. *Eukaryotic Cell*. 2013:12(6):776–793. https://doi.org/10.1128/ec.00318-12

Johnson JE, Berry JA. The role of cytochrome b_6f in the control of steady-state photosynthesis: a conceptual and quantitative model. *Photosynth Res*. 2021:148(3):101–136. https://doi.org/10.1007/s11120-021-00840-4

Johnson X, Steinbeck J, Dent RM, Takahashi H, Richaud P, Ozawa SI, Houille-Vernes L, Petroutsos D, Rappaport F, Grossman AR, et al. Proton gradient regulation 5-mediated cyclic electron flow under ATP- or redox-limited conditions: a study of Δ*ATPase pgr5* and

ΔrbcL pgr5 mutants in the green alga *Chlamydomonas reinhardtii*. *Plant Physiol*. 2014:165(1):438–452. https://doi.org/10.1104/pp.113.233593

Kaye Y, Huang W, Clowez S, Saroussi S, Idoine A, Sanz-Luque E, Grossman AR. The mitochondrial alternative oxidase from *Chlamydomonas reinhardtii* enables survival in high light. *J Biol Chem*. 2019:294(4):1380–1395. https://doi.org/10.1074/jbc.RA118.004667

Kramer DM, Evans JR. The importance of energy balance in improving photosynthetic productivity. *Plant Physiol*. 2011:155(1):70–78. https://doi.org/10.1104/pp.110.166652

Larosa V, Meneghesso A, La Rocca N, Steinbeck J, Hippler M, Szabò I, Morosinotto T. Mitochondria affect photosynthetic electron transport and photosensitivity in a green alga. *Plant Physiol*. 2018:176(3):2305–2314. https://doi.org/10.1104/pp.17.01249

Lemaire C, Wollman FA, Bennoun P. Restoration of phototrophic growth in a mutant of *Chlamydomonas reinhardtii* in which the chloroplast *atpB* gene of the ATP synthase has a deletion: an example of mitochondria-dependent photosynthesis. *Proc Natl Acad Sci U S A*. 1988:85(5):1344–1348. https://doi.org/10.1073/pnas.85.5.1344

Malone LA, Proctor MS, Hitchcock A, Hunter CN, Johnson MP. Cytochrome b_6f—orchestrator of photosynthetic electron transfer. *Biochim Biophys Acta*. 2021:1862(5):148380. https://doi.org/10.1016/j.bbabio.2021.148380

Mellon M, Storti M, Vera-Vives AM, Kramer DM, Alboresi A, Morosinotto T. Inactivation of mitochondrial complex I stimulates chloroplast ATPase in *Physcomitrium patens*. *Plant Physiol*. 2021:187(2):931–946. https://doi.org/10.1093/plphys/kiab276

Munekage Y, Hashimoto M, Miyake C, Tomizawa K-I, Endo T, Tasaka M, Shikanai T. Cyclic electron flow around photosystem I is essential for photosynthesis. *Nature*. 2004:429(6991):579–582. https://doi.org/10.1038/nature02598

Munekage Y, Hojo M, Meurer J, Endo T, Tasaka M, Shikanai T. PGR5 is involved in cyclic electron flow around photosystem I and is essential for photoprotection in *Arabidopsis*. *Cell*. 2002:110(3):361–371. https://doi.org/10.1016/S0092-8674(02)00867-X

Nawrocki WJ, Bailleul B, Picot D, Cardol P, Rappaport F, Wollman FA, Joliot P. The mechanism of cyclic electron flow. *Biochim Biophys Acta Bioenerg*. 2019:1860(5):433–438. https://doi.org/10.1016/j.bbabio.2018.12.005

Osmond CB. Photorespiration and photoinhibition: some implications for the energetics of photosynthesis. *Biochim Biophys Acta*. 1981:639(2):77–98. https://doi.org/10.1016/0304-4173(81)90006-9

Peltier G, Aro EM, Shikanai T. NDH-1 and NDH-2 plastoquinone reductases in oxygenic photosynthesis. *Ann Rev Plant Biol*. 2016:67(1):55–80. https://doi.org/10.1146/annurev-arplant-043014-114752

Peltier G, Schmidt GW. Chlororespiration—an adaptation to nitrogen deficiency in *Chlamydomonas reinhardtii*. *Proc Natl Acad Sci U S A*. 1991:88(11):4791–4795. https://doi.org/10.1073/pnas.88.11.4791

Peltier G, Tolleter D, Billon E, Cournac L. Auxiliary electron transport pathways in chloroplasts of microalgae. *Photosynth Res*. 2010:106-(1-2):19–31. https://doi.org/10.1007/s11120-010-9575-3

Petroutsos D, Terauchi AM, Busch A, Hirschmann I, Merchant SS, Finazzi G, Hippler M. PGRL1 participates in iron-induced remodeling of the photosynthetic apparatus and in energy metabolism in *Chlamydomonas reinhardtii*. *J Biol Chem*. 2009:284(47):32770–32781. https://doi.org/10.1074/jbc.M109.050468

Raghavendra AS, Padmasree K. Beneficial interactions of mitochondrial metabolism with photosynthetic carbon assimilation. *Trends Plant Sci*. 2003:8(11):546–553. https://doi.org/10.1016/j.tplants.2003.09.015

Rumberg B, Reinwald E, Schröder H, Siggel U. Correlation between electron flow, proton translocation and phosphorylation in chloroplasts. *Naturwissenschaften*. 1968:55(2):77–79. https://doi.org/10.1007/BF00599483

Saroussi SI, Wittkopp TM, Grossman AR. The type II NADPH dehydrogenase facilitates cyclic electron flow, energy-dependent quenching, and chlororespiratory metabolism during acclimation of *Chlamydomonas reinhardtii* to nitrogen deprivation. *Plant Physiol*. 2016:170(4):1975–1988. https://doi.org/10.1104/pp.15.02014

Schonbaum GR, Bonner WD Jr, Storey BT, Bahr JT. Specific inhibition of the cyanide-insensitive respiratory pathway in plant mitochondria by hydroxamic acids. *Plant Physiol*. 1971:47(1):124–128. https://doi.org/10.1104/pp.47.1.124

Shimakawa G, Ishizaki K, Tsukamoto S, Tanaka M, Sejima T, Miyake C. The Liverwort, Marchantia, drives alternative electron flow using a flavodiiron protein to protect PSI. *Plant Physiol*. 2017:173(3):1636–1647. https://doi.org/10.1104/pp.16.01038

Shimakawa G, Matsuda Y. Extra O_2 evolution reveals an O_2-independent alternative electron sink in photosynthesis of marine diatoms. *Photosynth Res*. 2024:159(1):61–68. https://doi.org/10.1007/s11120-023-01073-3

Stiehl HH, Witt HT. Quantitative treatment of the function of plastoquinone in photosynthesis. *Zeitschrift für Naturforschung B*. 1969:24(12):1588–1598. https://doi.org/10.1515/znb-1969-1219

Storti M, Alboresi A, Gerotto C, Aro E-M, Finazzi G, Morosinotto T. Role of cyclic and pseudo-cyclic electron transport in response to dynamic light changes in *Physcomitrella patens*. *Plant Cell Environ*. 2019:42(5):1590–1602. https://doi.org/10.1111/pce.13493

Storti M, Segalla A, Mellon M, Alboresi A, Morosinotto T. Regulation of electron transport is essential for photosystem I stability and plant growth. *New Phytol*. 2020:228(4):1316–1326. https://doi.org/10.1111/nph.16643

Strand DD, Fisher N, Kramer DM. The higher plant plastid NAD(P)H dehydrogenase-like complex (NDH) is a high efficiency proton pump that increases ATP production by cyclic electron flow. *J Biol Chem*. 2017:292(28):11850–11860. https://doi.org/10.1074/jbc.M116.770792

Takabayashi A, Kishine M, Asada K, Endo T, Sato F. Differential use of two cyclic electron flows around photosystem I for driving CO_2-concentration mechanism in C4 photosynthesis. *Proc Natl Acad Sci U S A*. 2005:102(46):16898–16903. https://doi.org/10.1073/pnas.0507095102

Tolleter D, Ghysels B, Alric J, Petroutsos D, Tolstygina I, Krawietz D, Happe T, Auroy P, Adriano JM, Beyly A, et al. Control of hydrogen photoproduction by the proton gradient generated by cyclic electron flow in *Chlamydomonas reinhardtii*. *Plant Cell*. 2011:23(7):2619–2630. https://doi.org/10.1105/tpc.111.086876

Tomaz T, Bagard M, Pracharoenwattana I, Lindén P, Lee CP, Carroll AJ, Ströher E, Smith SM, Gardeström P, Millar AH. Mitochondrial malate dehydrogenase lowers leaf respiration and alters photorespiration and plant growth in *Arabidopsis*. *Plant Physiol*. 2010:154(3):1143–1157. https://doi.org/10.1104/pp.110.161612

Treves H, Küken A, Arrivault S, Ishihara H, Hoppe I, Erban A, Höhne M, Moraes TA, Kopka J, Szymanski J, et al. Carbon flux through photosynthesis and central carbon metabolism show distinct patterns between algae, C3 and C4 plants. *Nat Plants*. 2022:8(1):78–91. https://doi.org/10.1038/s41477-021-01042-5

von Jagow G, Link TA. Use of specific inhibitors on the mitochondrial bc1 complex. *Methods in enzymology*. Vol. 126. Burlington, UK: Academic Press; 1986. p. 253–271.

Walker BJ, Strand DD, Kramer DM, Cousins AB. The response of cyclic electron flow around photosystem I to changes in photorespiration and nitrate assimilation. *Plant Physiol*. 2014:165(1):453–462. https://doi.org/10.1104/pp.114.238238